Equilibriumizing all food chain chaos through reproductive efficiency

Bo Deng
Department of Math and Statistics, University of Nebraska, Lincoln, Nebraska 68588-0323

(Received 31 May 2006; accepted 16 November 2006; published online 21 December 2006)

The intraspecific interference of a top-predator is incorporated into a classical mathematical model for three-trophic food chains. All chaos types known to the classical model are shown to exist for this comprehensive model. It is further demonstrated that if the top-predator reproduces at high efficiency, then all chaotic dynamics will change to a stable coexisting equilibrium, a novel property not found in the classical model. This finding gives a mechanistic explanation to the question of why food chain chaos is rare in the field. It also suggests that high reproductive efficiency of top-predators tends to stabilize food chains. © *2006 American Institute of Physics*.
[DOI: 10.1063/1.2405711]

Ecological chaos is rare but theoretical chaos is common in mathematical models of food chains. Because of the practical difficulty and cost associated with controlled field and laboratory experiments, studying how chaos arises and disappears from food chain models remains an attractive and economical way to understand these problems. In particular, such understandings may offer rare insights into the role that chaos plays in the evolution of predator-prey dynamics.

I. INTRODUCTION

The Rosenzweig-MacArthur food chain model has been used by many authors for food chain chaos, cf. Refs. 1–14. Our more recent work[15–18] shows that chaos occurs in a large region of parameter space of the Rosenzweig-MacArthur model, a result that, like many others, does not correlate well with empirical data.[19–22] The gap between the predicted and the observed was noticed in the late 1980s. A plausible explanation was proposed in Ref. 23, where it was hypothesized that the rarity of field food chain chaos is due to the fact that chaotic variations would inevitably drive down the species population to a too low level for the species to escape extinction. However, this explanation is not mechanistic, but phenomenological and circular. In other words, if ecological chaos is an evolutionary executioner, then what is the "capital" cause?

The purpose of this paper is to propose a mechanistic solution to the problem. The same approach has resolved a long list of theoretical problems in ecological research. All the problems arise from a subtle but critical defect of the classical Rosenzweig-MacArthur food chain model that does not include the effect of intraspecific competitions among predators. Without this consideration, the model inevitably leads to paradoxical predications, with the Enrichment Paradox, the Biological Control Paradox, and the Competition Exclusion Principle being the most notorious. See Ref. 24 for an early and direct field study contradicting the Enrichment Paradox assertion from Ref. 14. The issue of the Biological Control Paradox[25–28] was resolved in Ref. 29, which shows that the modified predator-prey model can indeed stabilize at an equilibrium point of arbitrarily small magnitude if the biological control agent can reproduce significantly faster than the pest. The Competitive Exclusion Principle fails to hold in general according to Ref. 30. All these artifacts disappear when intraspecific competition is taken into consideration for all species.

We will show that with the inclusion of intraspecific competition for the top-predator alone to the Rosenzweig-MacArthur food chain model, the "chaos paradox" effectively ceases to be an issue when the top-predator reproduces at high efficiency. In particular, *all* chaotic dynamics of the comprehensive model will bifurcate into a stable equilibrium with an increase in the top-predator's reproductive efficiency. The result thus suggests that reproductive inefficiency of species is an intrinsic cause of chaos-induced extinction, if such an evolutionary extinction scenario has ever happened, and that chaos is largely a theoretical spectacle for ecological systems since evolutionarily successful species are expected to be reproductively efficient. It also suggests to field and laboratory experimentalists that food chain chaos is likely to be found in systems of inefficient predators. The result further suggests that efficient top-predators are important for the stability of ecological systems.

The paper is organized as follows. We will introduce in Sec. II the modified Rosenzweig-MacArthur food chain model with the inclusion of intraspecific competitions of the predators. We will demonstrate in Sec. III how the food chain chaos mechanisms for the classical model extend to our comprehensive model. We will show in Sec. IV why all chaotic dynamics are eliminated by increasing the reproductive efficiency of the top-predator.

II. THE MODEL

Consider the following model for three-trophic food chains:

$$\dot{X} = rX\left(1 - \frac{X}{K}\right) - \frac{p_1 X}{H_1 + X}Y,$$

$$\dot{Y} = Y\left(\frac{b_1 p_1 X}{H_1 + X} - d_1 - s_1 Y\right) - \frac{p_2 Y}{H_2 + Y} Z, \tag{2.1}$$

$$\dot{Z} = Z\left(\frac{b_2 p_2 Y}{H_2 + Y} - d_2 - s_2 Z\right).$$

Here X, Y, Z are the densities for a prey, a predator, and a top-predator, respectively. Without predator Y, prey X is modeled by the logistic equation with r the maximum per capita growth rate and K the carrying capacity. Each predator is modeled according to Holling's type II disk function[31,32] with p_i the corresponding maximum per capita capture rate and H_i the semisaturation constant. Parameters b_1, b_2 are the birth-to-consumption ratios for the predators, the *reproductive efficiency* parameters mentioned in the Introduction. The products $b_i p_i$ are the maximum per capita reproductive rates of the predators. Each predator is subjected to a minimum per capita death rate d_i. It is assumed that each predator is in addition subjected to a density-dependent per capita death rate $s_1 Y, s_2 Z$, respectively, which may be interpreted to be the result of intraspecific competitions for resources. Without these two terms, the model is the classical Rosenzweig-MacArthur model[13] for food chains whose dynamics have been thoroughly analyzed.[4,6,9,10,12,15–18] As mentioned above, the exclusion of the predator's intraspecific interference in a two-species predator-prey model leads to predictions not supported by observations. The inclusion of these terms is further justified because it conforms to Verhulst's logistic growth principle.[32–35] This has been done for the two-species predator-prey system [with $Z=0$ in (2.1)] in Refs. 29 and 36.

For the purposes of capturing equivalent dynamics and simplifying mathematical analysis, the following changes of variables and parameters are used to transform the equations to a dimensionless form:

$$t \to b_1 p_1 t, \quad x = \frac{X}{K}, \quad y = \frac{Y}{Y_0}, \quad z = \frac{Z}{Z_0},$$

$$\text{with } Y_0 = \frac{rK}{p_1}, \quad Z_0 = \frac{b_1 rK}{p_2}, \tag{2.2}$$

$$\beta_1 = \frac{H_1}{K}, \quad \beta_2 = \frac{H_2}{Y_0}, \quad \delta_1 = \frac{d_1}{b_1 p_1}, \quad \delta_2 = \frac{d_2}{b_2 p_2},$$

$$\sigma_1 = \frac{s_1 Y_0}{b_1 p_1}, \quad \sigma_2 = \frac{s_2 Z_0}{b_2 p_2}, \quad \zeta = \frac{b_1 p_1}{r}, \quad \varepsilon = \frac{b_2 p_2}{b_1 p_1}.$$

The original idea that motivated this particular transformation can be found in Ref. 15. The same idea was used effectively in Refs. 16–18 as well. The new, dimensionless equations now become

$$\zeta \dot{x} = x\left(1 - x - \frac{y}{\beta_1 + x}\right) := xf(x,y),$$

$$\dot{y} = y\left(\frac{x}{\beta_1 + x} - \delta_1 - \sigma_1 y - \frac{z}{\beta_2 + y}\right) := yg(x,y,z), \tag{2.3}$$

$$\dot{z} = \varepsilon z\left(\frac{y}{\beta_2 + y} - \delta_2 - \sigma_2 z\right) := \varepsilon z h(y,z).$$

We only want to emphasize here that parameter $\zeta = b_1 p_1 / r$ is the YX prolificacy, measuring the maximum growth rate of Y against that of X. Similarly, parameter $\varepsilon = b_2 p_2 / (b_1 p_1)$ is the ZY-prolificacy parameter. By the theory of allometry,[37,38] these ratios correlate reciprocally well with the fourth roots of the ratios of X's body mass to Y's body mass, and, respectively, Y's body mass to Z's body mass. Thus ζ is usually of a small order. However, parameter ε may not be small in some biological control cases where the control agents are smaller in size than the pest species and reproduce faster. We also point out that 1 unit in the new dimensionless time scale equals $1/(b_1 p_1)$ units in the original time scale, which represents the average time interval between the birth of Y. This can be seen from the time scaling that $t \to \tau = b_1 p_1 t$ with τ being the new dimensionless time variable for which $\tau = 1$ corresponding to $t = \tau/(b_1 p_1) = 1/(b_1 p_1)$. To save notation, we simply retain t instead of τ for the new time variable in Eq. (2.3) as well as for the subsequent analysis below. Notice that at high reproductive efficiency for the top-predator (i.e., $b_2 \gg 1$), we have $\varepsilon = b_2 p_2 / (b_1 p_1) \gg 1$ when the other parameters are maintained at a normal or smaller magnitude.

The nondimensionalization reduces the number of parameters from 12 to 8, which means that the dynamics for the dimensionless equations at one set of parameter values is the same for the dimensional equations in a four-dimensional subspace of the dimensional parameter space.

For the analysis of this paper, we only consider the case of $0 < \zeta \ll 1$, which means the maximum reproductive per capita rate of X is faster than that of Y. Because of this, we can safely neglect Y's intraspecific interference effect and assume $s_1 = 0$. Detailed justifications were given in Ref. 29 for the predator-prey system without the top-predator Z. We will recall the justification argument later when we comment on Z's faster-than-Y's time scale with $\varepsilon \gg 1$.

III. CHAOS CONFIGURATIONS FOR $0 < \zeta \ll 1$, $0 < \varepsilon \ll 1$

In one respect, ecology is about the temporal rise and fall of species populations. It is known that the transition between these two phases takes place at nullclines of continuous population models. For the classical Rosenzweig-MacArthur food chain model, population oscillations, periodic or chaotic, are well understood by the time scale analysis (i.e., the singular perturbation method) based on the trophic time diversification hypothesis that the prey reproduces faster than the predator, which in turn reproduces faster than the top-predator; see Refs. 10, 12, and 15–18. The method organizes its classification scheme on the geometrical configuration of the nullclines.

The classification is possible because the number of geometrical configurations of the nullclines is finite. Two features are particularly helpful. (i) The trophic time diversification hypotheses, which allow the time scale parameters ζ, ε to be of various magnitudes, thus enabling a singular perturbation analysis of the dimensionless model. (ii) In the dimensionless form, the geometrical configurations of the nullclines are independent of the time scale parameters, fur-

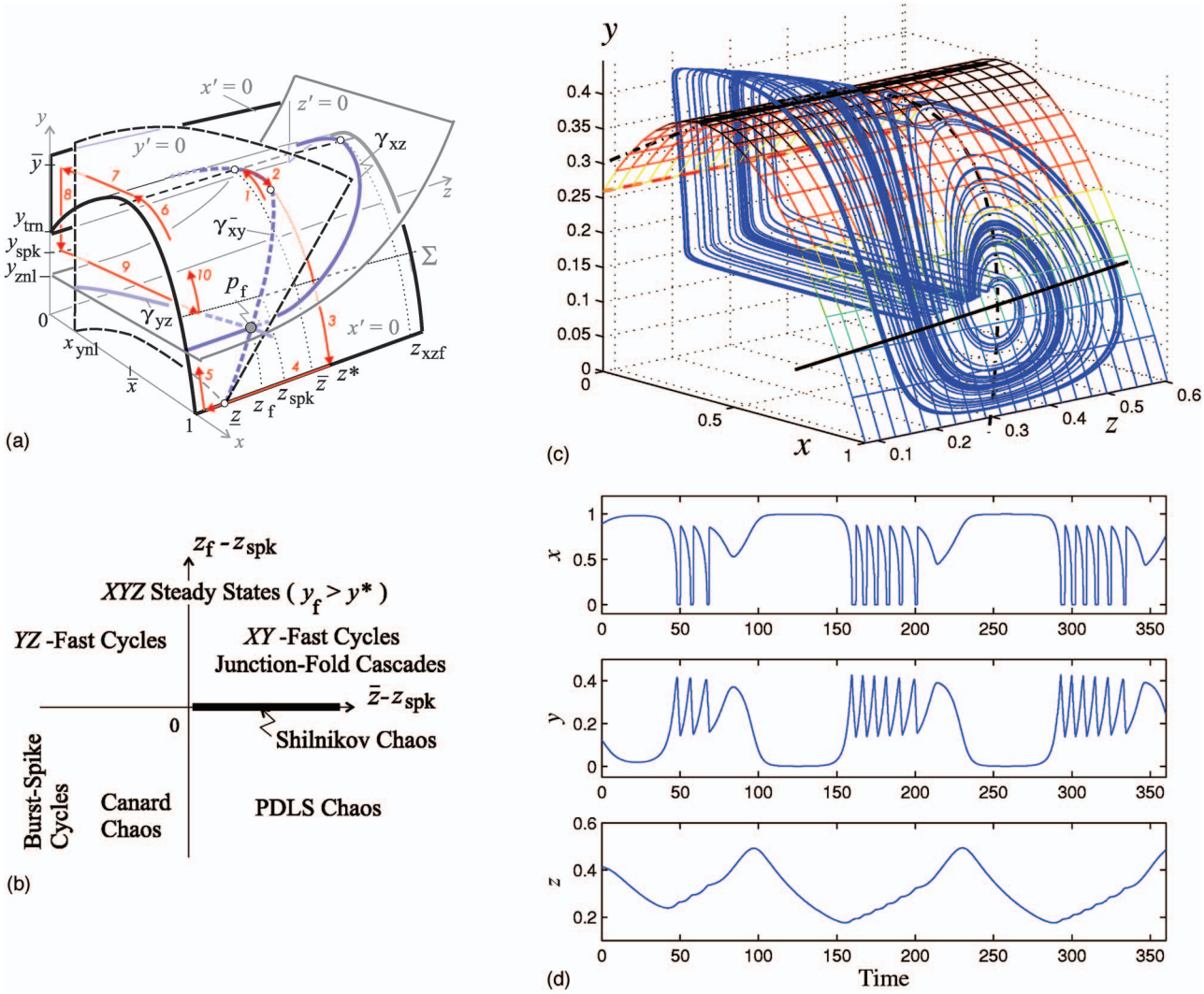

FIG. 1. (Color) (a) Nullcline surfaces. (b) Adapted from Ref. 18. (c) A typical teacup attractor. Parameter values are $\zeta=0.02$, $\varepsilon=0.375$, $\beta_1=0.26$, $\beta_2=0.5$, $\delta_1=0.2$, $\delta_2=0.18$, $\sigma_2=0.1$. (d) Typical time series of the attractor [over a truncated time interval of the attractor plot (c)].

ther simplifying the singular perturbation analysis. Figure 1(a) depicts the basic nullcline configurations for chaotic dynamics of Eq. (2.3). All technical details about the x and y nullclines can be found in Refs. 15–18 since they do not depend on the new parameter σ_2. We sketch below some of the qualitative properties that are needed for our discussion concerning $\sigma_2>0$. Our summary is under the conditions that the x variable changes the fastest $(0<\zeta\ll 1)$, the y variable does so the second fastest, and the z variable the slowest $(0<\varepsilon\ll 1)$.

Nullcline surfaces. The nontrivial x-nullcline surface, $f(x,y)=0$, is a cylindrical parabola parallel with the z axis. The fold of the surface ($f=0$, $f_x=0$) runs along the line $\{x=\bar{x}, y=\bar{y}\}$. It separates the surface into two parts. The part containing the prey's predator-free carrying capacity (1,0,0) consists of stable equilibrium points for the x equation, satisfying $f=0$, $f_x<0$. It represents the predator mediated carrying capacity for the prey. It decreases in x with an increase in y, i.e., more predators result in a smaller prey capacity. The other part that intersects the trivial x nullcline, $x=0$, consists of unstable equilibrium points of the x equation, satisfying $f=0$, $f_x>0$. It represents the predator-induced threshold for the prey: for each fixed y, an initial amount in x greater than the threshold leads the prey to its predator-mediated carrying capacity, and a smaller amount leads it to the extinction edge $x=0$. It increases in x with an increase in y. Hence these two parts must intersect and the intercept is the fold line, called the crash fold because for a slightly greater amount of y (but fixed), the prey subdynamics collapses to the extinction edge $x=0$ (orbit 7). We denote the capacity branch of the x nullcline by $\mathcal{S}_a$. The intersection of both trivial and nontrivial nullclines surfaces consists of transcritical points $\{x=0,\ y=y_{\rm trn}=\beta_1\}$, through which the phenomenon of Pontryagin's delay of loss of stability (PDLS) occurs.[17,39,40] The PDLS points corresponding to the crash fold line are denoted by $p_{\rm spk}$, with the y coordinate, $y_{\rm spk}$, of the points shown. Σ represents the PDLS points projected on the capacity surface $\mathcal{S}_a$ following the ζ-fast, x subflows (orbit 9). Roughly speaking, when originated from $y=\bar{y}$ and at the singular limit $\zeta\to 0$, the predator has to dip to the PDLS level $y_{\rm spk}<y_{\rm trn}$ to allow the prey to recover.

The nontrivial y-nullcline surface, $g(x,y,z)=0$, can be best described as a threshold surface for the y equation. For each fixed $x>x_{\rm ynl}=\beta_1\delta_1/(1-\delta_1)$, variable y increases with an increase in z on the surface. For y above it, the $y(t)$ subdynamics increases in t since $dy/dt=yg>0$ (orbits 1, 5, 6, 10) and for y below it the $y(t)$ subdynamics decreases in t toward $y=0$ since $dy/dt=yg<0$ (orbit 3). Its intersection with the capacity surface $\mathcal{S}_a$ of the x equation is the curve $\gamma_{\rm xy}$. This curve consists of two monotone parts when β_2 is small enough.[15] It has a maximum point in z, denoted by $p^*=(x^*,y^*,z^*)$. If one restricts the y equation on the x-capacity surface $\mathcal{S}_a$, then the part above y^*, $\gamma^+_{\rm xy}=\gamma_{\rm xy}\cap\{y>y^*\}$, is locally attracting for the y equation (orbit 1) when z is fixed, whereas the part below y^*, $\gamma^-_{\rm xy}=\gamma_{\rm xy}\cap\{y<y^*\}$, is locally repelling (orbit 3) because $\gamma_{\rm xy}$ separates $\mathcal{S}_a$ into two parts: above the y-nullcline surface where $g>0$ (orbits 5, 6, and 10) and below the y-nullcline surface where $g<0$ (orbit 3). In other words, the upper part is the top-predator mediated carrying capacity of y, and the lower part is the threshold. Both are supported by the x capacity $\mathcal{S}_a$. All in the z coordinate, the intersections of $\gamma_{\rm xy}$ with the predator-free capacity line $\{x=1,\ y=0\}$, the PDLS curve Σ, and the x-fold line $\{x=\bar{x},\ y=\bar{y}\}$ are $\underline{z}$, $z_{\rm spk}$, and $\bar{z}$, respectively, of which $\underline{z}$ is a y-transcritical point through which the PDLS phenomenon occurs for the y variable (orbits 3 and 5) if it has a faster maximum per capita reproductive rate than z does, which is the case under discussion in this section.

The nontrivial z-nullcline surface, $h(y,z)=0$, can be solved as $z=[y/(\beta_2+y)-\delta_2]/\sigma_2$. It degenerates to a plan $y=y_{\rm znl}=\beta_2\delta_2/(1-\delta_2)$ at $\sigma_2=0$. For $\sigma_2>0$, variable z increases on the surface with an increase in $y>y_{\rm znl}$. As y tends to ∞, variable z saturates toward $(1-\delta_2)/\sigma_2$. For each fixed $y>y_{\rm znl}$, this surface consists of attracting equilibrium points for the z equation because $h_z<0$ [Fig. 2(a)]. In particular, above the surface $dz/dt>0$ (orbit 2) and below it $dz/dt<0$ (orbit 4). For this reason, it can be considered as the carrying capacity of the top-predator supported by the middle predator. The intersection of this surface with the x-nullcline surface is the curve $\gamma_{\rm xz}$. The intersection of $\gamma_{\rm xz}$ with x's fold line $\{x=\bar{x},\ y=\bar{y}\}$ is $z_{\rm xzf}$ in the z variable, as shown. Its intersection with the xy-nullcline curve $\gamma_{\rm xy}$ is an xyz-equilibrium point. It is easy to see that for $y_{\rm znl}<\bar{y}$ and σ_2 sufficiently small, the intersection is unique, denoted by $p_{\rm f}$. The intersection of the z-capacity surface ($h=0$) with the y-threshold surface ($g=0$) is the curve $\gamma_{\rm yz}$ shown. In fact, we can make the following precise statement.

Proposition 3.1. *Let $y_*=y_{\rm znl}+\beta_2/1-\delta_2$. Then under the condition that $y_*<y_{\rm trn}=\beta_1$, there is a constant σ_2^* so that for $0<\sigma_2<\sigma_2^*$, $\gamma_{\rm yz}$ is monotone in x and y, and $\gamma_{\rm xy}$, $\gamma_{\rm xz}$, $\gamma_{\rm yz}$ intersect at a unique xyz equilibrium point $p_{\rm f}$.*

Proof. Notice first that the intersection of $\gamma_{\rm xz}$ and $\gamma_{\rm yz}$ is automatically on $\gamma_{\rm xy}$. Hence we only need to restrict all the curves on the z nullcline $h=0$, in particular the first two $\gamma_{\rm xz}$, $\gamma_{\rm yz}$. Notice also that the z nullcline $z=[y/(\beta_2+y)-\delta_2]/\sigma_2$ increases with an increase in $y>y_{\rm znl}$ and is parallel to the x axis. Therefore, we can project both curves to the xy plane and their configurations will uniquely determine the configurations in the full 3-space. To this end, the projected $\gamma_{\rm xz}$ curve looks exactly the same as the parabola $f(x,y)=0$ since the x nullcline is independent of z. For the $\gamma_{\rm yz}$ curve, it is equivalently defined as $Q(x,y)=x/\beta_1+x-q(y)=0$ with $q(y)=\delta_1+1/\beta_2+y[y/\beta_2+y-\delta_2]/\sigma_2$ after eliminating the variable z from both $g=0$ and $h=0$, from which x can be solved as $x=\beta_1 q(y)/[1-q(y)]$. From here it is straightforward to show the following. We have the partial derivatives $Q_x>0$ and $Q_y=0$ at only one possible point, $y_*=y_{\rm znl}+\beta_2/1-\delta_2$. In addition, x has a horizontal asymptote at the smallest y value $y_{\rm a}>y_{\rm znl}$ such that $1-q(y_{\rm a})=0$, and at any solution of $1-q(y)=0$ for that matter. To make sure y_* is not in the domain of $\gamma_{\rm yz}$, we only need $y_*>y_{\rm a}$ or $1-q(y_*)<0$, which solves for $\sigma_2<(1-\delta_2)/[(2\beta_2+1-\delta_2)(1-\delta_1)]:=\sigma_2^*$. Thus the $\gamma_{\rm yz}$ curve is bounded between $y_{\rm znl}$ and $y_{\rm a}$, strictly increasing without bound in x as y approaches $y_{\rm a}$. Moreover, the y range is bounded blow $y_{\rm trn}$ under the assumption that $y_*<y_{\rm trn}$. Thus, the curve $\gamma_{\rm yz}$ can intersect only the portion of $\gamma_{\rm xz}$ below the point $y_{\rm trn}$, which is monotone decreasing in x. Hence, there must be an intersection because $x_{\rm ynl}<1$ and the intersection is unique, which is the unique equilibrium point $p_{\rm f}$.

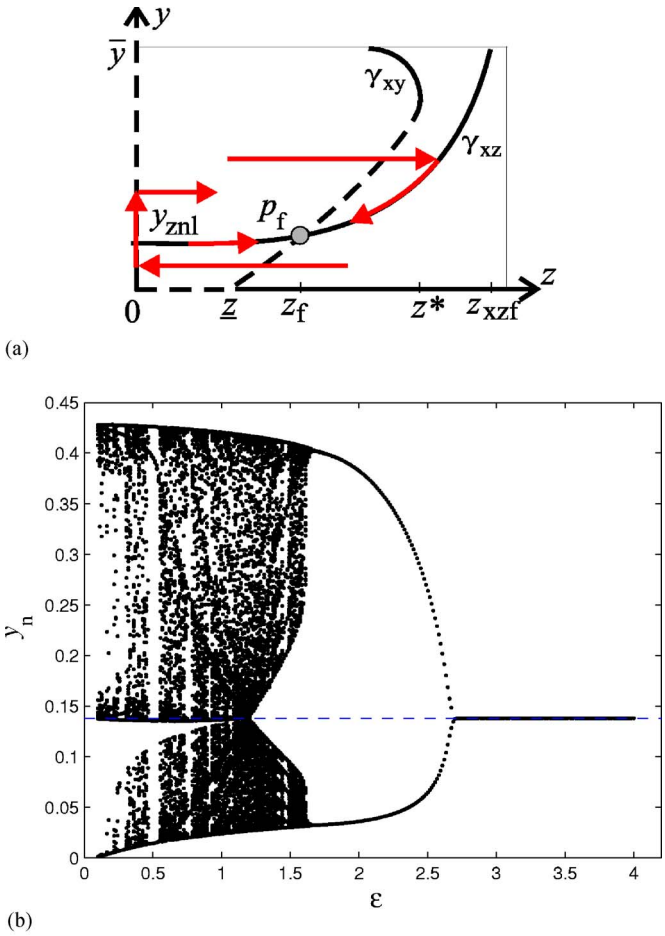

FIG. 2. (a) A singular phase portrait in the yz equation on the capacity surface of the x nullcline $f=0$. All ε-fast singular orbits converge to the equilibrium point regardless of the geometric configurations. (b) A sample bifurcation diagram in variable y and parameter ε. The chaos dynamics starts with a teacup attractor at the small end of ε. The dashed line is the equilibrium point branch, which stays constant for all ε since the nullcline surfaces do not change with ε. Parameter values other than ε are the same as Fig. 1(c).

[Note that since the γ_{yz} is attracting for the y equation for each fixed $x>x_{ynl}$ (with $g<0$ above the curve and $g>0$ below it) when the equations are restricted on the z-capacity surface, the curve represents the carrying capacity of y, supported by x and mediated by z.] □

Food chain chaos types. Because of this result, the geometric configurations considered in Refs. 15–18 for $\sigma_2=0$ hold for the system for $0<\sigma_2<\sigma_2^*$ and $y_*<\beta_1$. Hence, all food chain chaos types known for this model from the previously cited studies persist for the case $0<\sigma_2<\sigma_2^*, y_*<\beta_1$ with the trophic time diversification condition that $0<\zeta\ll 1, 0<\varepsilon\ll 1$. More specifically, the results are summarized in Fig. 1(b). They are organized according to the auxiliary parameters $u:=\bar{z}-z_{spk}, v:=z_f-z_{spk}$. The illustration is for the singular case when $\zeta=0$ and $0\leqslant\varepsilon\ll 1$. The Shilnikov chaos case is a minor exception for which $\varepsilon\sim O(1)$. Detailed descriptions about the junction-fold chaos[5] can be found in Ref. 15; those about the Shilnikov chaos[9] in Ref. 16; PDLS chaos in Ref. 17; and canard chaos (a.k.a. teacup chaos from Ref. 4) and burst-spike cycles[6,8] in Ref. 18. The remaining nonchaotic dynamics can be found in Ref. 10, whose parameter region is indeed smaller than the chaotic ones combined. Here is how to read Fig. 1(b). As an example, for parameter values satisfying $u=\bar{z}-z_{spk}>0, v=z_f-z_{spk}<0$, the singular asymptotic attractor for $\zeta=0$ and $0\leqslant\varepsilon\ll 1$ is a PDLS attractor as indicated. Figure 1(c) illustrates a sample canard chaos for the new system with $0<\zeta\ll 1$. It is qualitatively similar to its counterpart from Ref. 18, yet γ_{xz} is clearly not a flat line like the unperturbed system with $\sigma_2=0$.

Reproduction time scale, population boom and bust dynamics. To link these illustrations together, we use the canard chaos attractor [Fig. 1(c)] as an example. Solutions on the attractor for the perturbed case $0<\zeta\ll 1, 0<\varepsilon\ll 1$ [Fig. 1(c)] are approximated by the so-called singular solutions for the unperturbed case $\zeta=0, \varepsilon=0$ [Fig. 1(a)], and the limiting attractor persists in the form of so-called singular attractors. Flow lines 1 through 10 in Fig. 1(a) are examples of the typical singular orbits at the limit $\zeta\to 0$, $\varepsilon\to 0$.

In particular, if a point is not on the x nullcline, the singular x solution, such as orbits 7 and 9, with fixed y, z will take it quickly either to the trivial branch $x=0$ or the capacity branch $\mathcal{S}_a$. In other words, the prey density will quickly *equilibriumize* if it reproduces faster than all predators. But the equilibriumization often does not last, such as orbits 6 and 8. More specifically, the x-fast orbit 7 follows 6 because a high y induces a crash in x while orbit 9 follows 8 because a low enough y permits a rebound in x. The severity of crash and the vitality of rebound depend on the relative reproductive time scales. The smaller the ζ, the harsher the crash, and, respectively, the faster the rebound. In reality though, the species may not have a chance to rebound if a crash preceding it is too severe to prevent the species from extinction due to some exogenous factors that would otherwise be insignificant when the species is at its capacity state.

Once it is on the attracting part of the x nullcline, the y equation restricted on the x-nullcline surface takes over and the singular solution with fixed z but changing x according to $x=0$ or $f(x,y)=0$ will develop toward the attracting part of the y nullcline, such as orbits 1, 3, 5, 6, 8, and 10. That is, it is the predator's turn to equilibriumize. Again, some do not last, such as orbits 2 and 4. Also, population collapse may occur, orbit 3, before it can rebound, orbit 5.

Once it is on the attracting part of the xy nullcline, γ_{xy} or $\{x=1, y=0\}$, the xy-nullcline restricted z equation finally takes over, and ε-slow orbits such as 2 and 4 take the singular orbit either to the y-crash point p^* to start orbit 3 or through the y-transcritical point $\underline{z}$ and to the corresponding PDLS point to start orbit 5. In this case, a crash in z, orbit 4, follows a crash in y, orbit 3. The top-predator rebound is build on the xy cycles, such as orbits 6 through 10, which are themselves perilous if ζ is large while the nullcline surfaces remain the same.

It is in this singular limiting sense that the partition of the parameter space by Fig. 1(b) holds not only for $\zeta=0, 0\leqslant\varepsilon\ll 1$ but also qualitatively so for $0<\zeta\ll 1$, $0\leqslant\varepsilon\ll 1$. Figure 1(d) illustrates the effects of the time scales $0<\zeta\ll 1, 0<\varepsilon\ll 1$ on the time series of the systems. The fast spikes seen on the x,y time series are due to x's fastest time scale with $0<\zeta\ll 1$. The sharp initiation and termination of the spikes are due to y's fast time scale next to x's because of $0<\varepsilon\ll 1$. The long, slow transients between the bursts of fast spikes are due to z's slow time scale. As pointed out earlier, such exotic oscillations may not be observable because a population bust can terminate the spectacle prematurely.

IV. EQUILIBRIUMIZATION FOR $\varepsilon\gg 1$

The time scales $0<\zeta\ll 1, 0<\varepsilon\ll 1$ are not only an integral part of the chaos generation mechanisms outlined above, but also an integral part of the singular perturbation method by which the chaotic dynamics are established. Once the time scale is reversed to $\varepsilon\gg 1$, instead of developing in the y direction first on $\mathcal{S}_a$, the $\mathcal{S}_a$ constrained yz subdynamics will develop in the z direction first. Figure 2(a) illustrates the singular dynamics under this inverted time scale. Notice that the nontrivial z nullcline, γ_{xz}, is a monotone increasing curve if and only if $\sigma_2>0$, and the point $(y_{znl},0)$ is a transcritical point for the z equation through which the PDLS phenomenon will occur. We can now see that the ε-fast orbits are lines parallel to the z axis, which will eventually converge to the equilibrium point. In fact, if an initial point lies above $y=y_{znl}$, it will converge to the z nullcline right away. On the z-capacity curve γ_{xz}, the ε-slow y dynamics takes over, leading the singular orbit to the equilibrium point. If the initial point lies below $y=y_{znl}$, the ε-fast orbit goes to $z=0$ first. Then the ε-slow y flow takes over and passes through the transcritical point. At its corresponding PDLS point, predator y recovers to a high enough value to allow the top-predator to initiate a population boom, taking the orbit to the z-capacity branch γ_{xz}, and eventually to the equilibrium point. That is, all singular orbits converge to the coexisting equilibrium point p_f. In fact, the local stability of the equilibrium point can be analyzed precisely as follows.

Proposition 4.1. *For sufficiently large $\varepsilon\gg 1$, the unique equilibrium point p_f is stable for the reduced yz subsystem on x's capacity surface $\mathcal{S}_a$.*

Proof. A proof can be obtained similar to Ref. 29. Let

$y'=yg(\phi(y,z),y,z):=G(y,z), z'=\varepsilon z h(z,y):=\varepsilon H(y,z)$ be the yz equations restricted on the x-capacity surface $\mathcal{S}_a$, with $x=\phi(y,z)$ representing $\mathcal{S}_a$. Let $u=y-y_p, v=z-z_p$ and the linearized equations at the equilibrium point be

$$\dot{u}=G_1u+G_2v, \quad \dot{v}=\varepsilon H_1u+\varepsilon H_2v, \tag{4.1}$$

where $G_1=\partial G/\partial y$ is evaluated at the yz-equilibrium point and so on. The corresponding u nullcline $G_1u+G_2v=0$ is the tangent line to the y nullcline γ_{xy} at the equilibrium point. Thus the slope $-G_1/G_2>0$ if the equilibrium point is on the threshold branch γ_{xy}^- and $-G_1/G_2<0$ if it is on the capacity branch γ_{xy}^+. Since linearization G_1u+G_2v preserves the same qualitative property as $dy/dt=G(y,z)$ for which $G<0$ for large z, we have $G_1u+G_2v<0$ for large v, implying $G_2<0$. Hence, $G_1>0$ if and only if the equilibrium point is on the threshold branch γ_{xy}^-.

Similarly, $H_1>0$, $H_2<0$ no matter where the equilibrium is since the line $H_1u+H_2v=0$ mirrors the z nullcline and $H_1u+H_2v<0$ for large v to mirror the qualitative property that $dz/dt<0$ for large z. The property that $H_1>0$ follows from the property that γ_{xz} is always increasing in z when y increases.

These conditions imply the following. If the equilibrium point is on y's capacity branch ($G_1<0$), it is *always* stable.[29] If the equilibrium point is on y's threshold branch, with $G_1>0$, then the slope of the v nullcline must be greater than the slope of the u nullcline, $-H_1/H_2>-G_1/G_2$, because of the same manner in which γ_{xz} and γ_{xy} intersect, see Fig. 1(b). Using this property, it is straightforward to show that for

$$\varepsilon>-\frac{G_1}{H_2},$$

the eigenvalues

$$[(\varepsilon H_2+G_1)\pm\sqrt{(\varepsilon H_2+G_1)^2-4\varepsilon(G_1H_2-G_2H_1)}]/2$$

of Eq. (4.1) always have a negative real part. Moreover, by decreasing ε, the eigenvalues will cross the imaginary axis (when $\varepsilon H_2+G_1=0$) so that the stable equilibrium point will give way to a stable limit cycle via Hopf bifurcation. □

We now note that without the $\sigma_2>0$ term, the xz nullcline γ_{xz} is a line parallel with the z axis, which will lead to a well-known problem for the z subsystem under the condition that z has a faster time scale than y does with $\varepsilon\gg 1$. In fact, if $\sigma_2=0$, then for any fixed $y>y_{znl}$, the z-fast solution $z(t)$ grows exponentially without bound as $t\to\infty$ since $dz/dt=\varepsilon z h(y,0)>0$, the classical Malthusian fallacy against Verhulst's logistic principle.

Figure 2(b) is a bifurcation diagram in y versus ε. The map is generated from points at which the orbit hits the nontrivial y nullcline $g(x,y,z)=0$, that is, whenever the solution in y is either a local maximum or a local minimum. Tracing the diagram leftward, we first encounter the stable coexisting equilibrium state at parameter ε's high end. At a smaller $\varepsilon\sim 2.65$, it loses its stability and undergoes a Hopf bifurcation. This periodic orbit grows until it hits the x-crash-fold near $\varepsilon\sim 1.65$, an event of crisis, exploding to a chaotic attractor that then changes to contain a chaotic Shilnikov's orbit[16] near $\varepsilon\sim 1.2$, at which the equilibrium point is part of the attractor, and eventually becomes a teacup type at the lower end of ε. Notice that the stabilizing parameter range in ε is in fact quite moderate. It will become more so if the other time scale ζ is relaxed further from $\zeta=0$. More importantly, the identical equilibriumization process at large ε holds for all other nullcline configurations from Fig. 1(b), and all parameter regions of distinct dynamics, chaotic or otherwise, will emerge into one region of stable equilibrium for sufficiently large ε. Furthermore, all $\varepsilon\sim\infty$ singular orbits converge to the equilibrium point p_f as shown in Fig. 2(a), which in turn gives a theoretical explanation as to why the relaxed equilibrium appears globally stable in the bifurcation diagram Fig. 2(b).

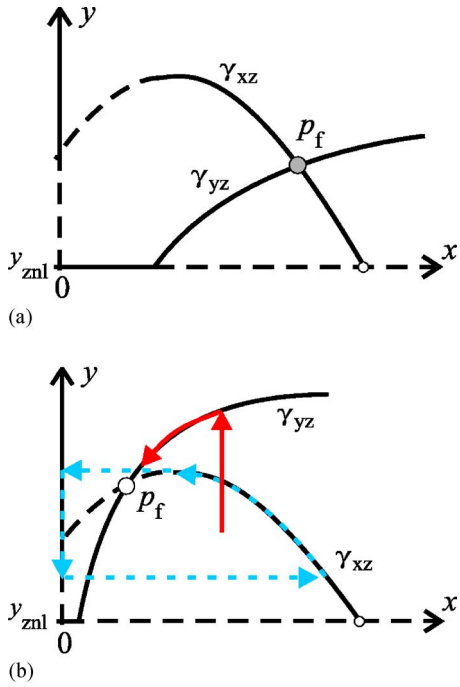

FIG. 3. Nullclines of the xy equations restricted on the capacity surface of the z nullcline $\{h(y,z)=0, y>y_{znl}\}$ when z has the fastest reproducing time scale. (a) The case with p_f on $\mathcal{S}_a$. (b) The other case with p_f on the x-threshold surface.

V. DISCUSSION

Taking the time scale to the extreme that z has the fastest reproducing time scale, $b_2p_2\gg r\gg b_1p_1$, i.e., $\varepsilon\gg 1/\zeta$, the same equilibriumization phenomenon persists, which is illustrated in Fig. 3(a). Here, all singular orbits are first equilibriumized to the capacity surface of the z nullcline $\{h=0\}$, and the subsequent development is determined by the xy equation restricted on the surface. The reduced xy dynamics is a typical predator-prey interaction that can be completely determined by the configuration of the z-mediated nullclines γ_{xz} and γ_{yz}. In fact, as we demonstrated in Proposition 1, the yz nullcline γ_{yz} increases in y as x increases and it intersects the xz nullcline γ_{xz} at a unique point on the x capacity part of the curve $\mathcal{S}_a$, as shown. The proof given above for Proposition (4.1) as well as Ref. 29 shows that regardless of the time scale with respect to ζ, such an equilibrium point p_f is always stable.

For the case in which p_f is not on $\mathcal{S}_a$, it is easy to show that the only possible singular attractors are xy-fast cycles, and no limiting chaos attractors exist. In fact, in the extreme case of z having the fastest time scale, the xy subdynamics restricted on z's capacity surface $\{h=0\}$ is illustrated in Fig. 3(b), for which condition $0<\zeta\ll 1$ will give rise to a limit cycle (dashed arrow lines), and condition $\zeta\gg 1$ will lead to a stable equilibrium point (solid arrow lines) by the same equilibriumization process described here and in Ref. 29. For the remaining cases in which $\sigma_2>\sigma_2^*, \sigma_1\geqslant 0$, no matter how complex the full three-dimensional dynamics is, at the singular limit $\varepsilon\to\infty$ the approximating dynamics is the two-dimensional xy dynamics on the capacity z nullcline for which the most complex structure has the form of limit cycles only.

In terms of its dimensional parameters, $\varepsilon=b_2p_2/(b_1p_1)$. For ε to be modestly large, b_2p_2 is modestly large relative to b_1p_1. For b_2p_2 to be modestly large, the top-predator either catches more preys per capital (p_2 large) or reproduces more per catch (b_2 large), or it does both. It is clear then that the top-predator is quantifiably efficient if it is reproductively efficient with a greater birth-to-consumption ratio b_2. We note that with other dimensional parameters fixed, increasing b_2 will not change the nullcline structures of the XY subchain below.

We now see that because of the role the reproductive efficiency b_2 plays in the analysis above and because of the modest magnitude of ε by which the chain stabilization occurs (Fig. 2), our result indeed suggests a general, albeit theoretical, principle that increasing top-predator's reproductive efficiency tends to stabilize the whole food chain. An important implication is that ecological stability is the result of reproductive efficiency—a product of evolutionary optimization.

[1] M. P. Boer, B. W. Kooi, and S. A. L. M. Kooijman, "Homoclinic and heteroclinic orbits to a cycle in a tri-trophic food chain," J. Math. Biol. **39**, 19–38 (1999).
[2] O. De Feo and S. Rinaldi, "Singular homoclinic bifurcations in tritrophic food chains," Math. Biosci. **148**, 7–20 (1998).
[3] O. De Feo and S. Rinaldi, "Top-predator abundance and chaos in tritrophic food chains," Ecol. Lett. **2**, 6–10 (1999).
[4] A. Hastings and T. Powell, "Chaos in a three-species food chain," Ecology **72**, 896 (1991).
[5] P. Hogeweg and B. Hesper, "Interactive instruction on population interactions," Comput. Biol. Med. **8**, 319–327 (1978).
[6] Y. A. Kuznetsov and S. Rinaldi, "Remarks on food chain dynamics," Math. Biosci. **133**, 1–33 (1996).
[7] Yu. A. Kuznetzov, O. De Feo, and S. Rinaldi, "Belyakov homoclinic bifurcations in a tritrophic food chain model," SIAM J. Appl. Math. **62**, 462–487 (2001).
[8] L. Lenbury and C. Likasiri, "Low- and high-frequency oscillations in a food chain where one of the competing species feeds on the other," Math. Comput. Modell. **20**, 71–89 (1994).
[9] K. McCann and P. Yodzis, "Bifurcation structure of a three-species food chain model," Theor Popul. Biol. **48**, 93–125 (1995).
[10] S. Muratori and S. Rinaldi, "Low- and high-frequency oscillations in three-dimensional food chain system," SIAM J. Appl. Math. **52**, 1688–1706 (1992).
[11] V. Rai and W. M. Schaffer, "Chaos in ecology," Chaos, Solitons Fractals **12**, 197–203 (2001).
[12] S. Rinaldi and S. Muratori, "Slow-fast limit cycles in predator-prey models," Ecol. Modell. **61**, 287–308 (1992).
[13] M. L. Rosenzweig and R. H. MacArthur, "Graphical representation and stability conditions of predator-prey interactions," Am. Nat. **97**, 209–223 (1963).
[14] M. L. Rosenzweig, "Paradox of enrichment: Destabilization of exploitation ecosystems in ecological time," Science **171**, 385–387 (1971).
[15] B. Deng, "Food chain chaos due to junction-fold point," Chaos **11**, 514–525 (2001).
[16] B. Deng and G. Hines, "Food chain chaos due to Shilnikov orbit," Chaos **12**, 533–538 (2002).
[17] B. Deng and G. Hines, "Food chain chaos due to transcritical point," Chaos **13**, 578–585 (2003).
[18] B. Deng, "Food chain chaos with canard explosion," Chaos **14**, 1083–1092 (2004).
[19] M. P. Hassell, J. H. Lawton, and R. M. May, *Patterns of dynamical behaviour in single-species populations*, J. Anim. Ecol. **45**, 471–486 (1976).
[20] W. R. Thomas, M. J. Pomerantz, and M. E. Gilpin, "Chaos, asymmetric growth and group selection for dynamical stability," Ecology **61**, 1312–1320 (1980).
[21] J. A. Logan and J. C. Allen, "Nonlinear dynamics and chaos in insect populations," Annu. Rev. Entomol. **37**, 455–477 (1992).
[22] S. Ellner and P. Turchin, "Chaos in a noisy world: New methods and evidence from time-series analysis," Am. Nat. **145**, 343–375 (1995).
[23] A. A. Berryman and J. A. Millstein, "Are ecological systems chaotic—and if not, why not?," Trends Ecol. Evol. **4**, 26–28 (1989).
[24] C. D. McAllister and R. J. LeBrasseur, "Stability of enriched aquatic ecosystems," Science **175**, 562–565 (1971).
[25] R. F. Luck, "Evaluation of natural enemies for biological control: A behavior approach," Trends Ecol. Evol. **5**, 196–199 (1990).
[26] P. A. Abrams, "The fallacies of 'ratio-dependent'," Ecology **75**, 1842–1850 (1994).
[27] H. R. Kcakaya, R. Arditi, and L. R. Ginzburg, "Ratio-dependent predation: An abstraction that works," Ecology **76**, 995–1004 (1995).
[28] M. Astrom, "The paradox of biological control revisited: Per capita nonlinearities," Oikos **78**, 618–621 (1997).
[29] B. Deng, S. Jessie, G. Ledder, A. Rand, and S. Srodulski, "Biological control does not imply paradox," J. Math. Biosciences (to be published).
[30] I. Loladze, Y. Kuang, J. J. Elser, and W. F. Fagan, "Competition and stoichiometry: Coexistence of two predators on one prey," Theor Popul. Biol. **65**, 1–15 (2004).
[31] C. S. Holling, "Some characteristics of simple types of predation and parasitism," Can. Entomol. **91**, 385–398 (1959).
[32] T. Royama, "A comparative study of models for predation and parasitism," Researches Popul. Ecol. Kyoto Univ. Suppl. **1**, 1–91 (1971).
[33] P. F. Verhulst, "Notice sur la loi que la population suit dans son accroissement," Corr. Math. Phys. **10**, 113–121 (1838).
[34] A. J. Lotka, *Elements of Physical Biology* (Williams and Wilkins, Baltimore, MD, 1925).
[35] V. Volterra, "Fluctuations in the abundance of species, considered mathematically," Nature **118**, 558–560 (1926).
[36] A. D. Bazykin, *Nonlinear Dynamics of Interacting Populations*, edited by A. I. Khibnik and B. Krauskopf (World Scientific, Singapore, 1998).
[37] W. A. Calder III, "An allometric approach to population cycles of mammals," J. Theor. Biol. **100**, 275–282 (1983).
[38] W. A. Calder III, "Ecological scaling: Mammals and birds," Annu. Rev. Ecol. Syst. **14**, 213–230 (1983).
[39] L. C. Pontryagin, "Asymptotic behavior of solutions of systems of differential equations with a small parameter at higher derivatives," Izv. Akad. Nauk SSSR, Ser. Mat. **21**, 605–626 (1957) (in Russian).
[40] S. Schecter, "Persistent unstable equilibria and closed orbits of a singularly perturbed equation," J. Differ. Equations **60**, 131–141 (1985).